Generation of Frequency Dependent Chaos using Single Transistor in 180nm CMOS Technology

Sai Venkatesh Balasubramanian

Sree Sai Vidhya Mandhir, Mallasandra, Bengaluru-560109, Karnataka, India.
saivenkateshbalasubramanian@gmail.com

Abstract

A frequency dependant chaos generator offering the twin advantages of simplicity of implementation and easy control and tunability is proposed using an iterative map based on the circle map and characterized using bifurcation diagrams. The nonlinearity of a single MOS transistor is effectively harnessed and is used to design a frequency dependant chaos generator using ring oscillators for the driving signals. The proposed design is implemented at the deep submicron VLSI level at 180nm CMOS Technology using SPICE Simulation. The generated chaos is characterized qualitatively using waveforms, spectra and phase portrait. Quantitative characterization using Lyapunov Exponent, Kolmogorov Entropy and Fractal Dimension ascertain the chaotic nature. Finally, the dependance of the nature of chaos generated on the power supply and on the driving signal frequency is characterized. The simplicity of circuitry coupled with the frequency dependence and low power dissipation form the key highlights of the present work. The chaotic signal generated in the present work serve as a potential candidate as a carrier in secure communication systems and encryption techniques.

Keywords: Frequency Dependent Chaos, Ring Oscillator, 180nm CMOS

1. Introduction

The advancement of computing and storing power in recent years, coupled with the ability to simulate complex systems and visualize their long-term evolution patterns has brought to the limelight, the flagship of nonlinear science, Chaos Theory [1, 2]. The principal premises of chaos theory have been determinism and an extremely sensitive dependence on initial conditions [3, 4, 5]. Chaos theory has found success in being able to model and study various systems occurring in nature such as celestial mechanics, biological systems including the electrical activity of the heart and the brain, various chemical reactions, spread of epidemics, weather patterns and so on [4, 3, 6].

In the field of electronics and semiconductors, the introduction of a nonlinear element such as the Chua diode have enabled considerable progress in generating a wide variety of chaotic signals, modeling classical systems such as the Lorenz Attractor and the Rossler Attractor [5]. This generation of chaos has found immediate and significant application in establishing secure communication systems, which exhibit significant security enhancing properties, thanks to the sensitivity property of chaos [7, 8].

The present work purports to the definition and the generation of a new kind of chaos where the chaotic parameter is not amplitude or phase as conventionally seen, but frequency [4, 6]. The advantages of frequency dependent chaos are twofold. Firstly, it makes use of any signal naturally being decomposed into a set of frequencies. This leads to easy implementation using a single transistor as the chaotic 'system', since the nonlinearity proposed in the frequency dependant chaos is the natural switching operation of the transistor [9]. Secondly, having frequency as the control parameter makes it possible to tune the system, which enables a signal based control, a marked deviation from the system defined control typically seen in chaotic systems [4].

The proposed frequency dependant chaos is characterized using the iterative map and bifurcation diagrams. Then, an extremely simple circuit generating such a chaotic signal is designed and implemented in deep sub-micron VLSI layout design at 180nm using SPICE simulations [10, 11, 12]. The essential parts of the system are ring oscillators to generate the driving signals, and a single NMOSFET as the nonlinear element. The factor of tunability comes due to the possibility of changing the frequency input to the single NMOSFET by altering the number of ring oscillator stages. In order to physically achieve this, a 'programmable ring oscillator' can be used where the number of stages actually in the ring can be switched. The generated chaos is characterized using various standard techniques such as the Lyapunov Exponent, Kolmogorov Entropy and Fractal Dimension. The principal advantage of using an extremely simple circuit to generate chaos is the low value of power dissipation obtained, and this is studied using a parametric analysis [10].

It is noteworthy that generation of chaos using ring oscillators have been reported in literature [13, 14, 15, 16, 17, 18]. It is seen that the basic structure of two ring oscillators being used coupled with a nonlinear circuit gives rise to chaotic behavior. However, the design proposed in the present work differs from such results in the key aspect of frequency dependance, which can be obtained by altering the number of stages in a ring oscillator. This factor, coupled with the extremely simple circuitry and low power dissipation form the key highlights of the present work.

2. Formulation of the Frequency Dependent Chaos

The first step in the formulation of any chaotic system is an iterative map, a relation describing how a 'chaotic' parameter of the system evolves with time with respect to a control parameter r [4]. In the present work, the chaotic parameter is frequency, rather than amplitude or phase. This offers the twin advantages of simple circuitry and tunability and control, as mentioned earlier.

The present work purports to designing a system that is able to generate chaos as a result of nonlinear interactions between two oscillations with competing frequencies. It has been well established in literature that circle maps are ideally suited to describing such systems [19, 20, 21, 22, 23]. Hence, the iterative function proposed in the present work is inspired from the standard circle map, whose iterative map is given as follows [19, 20]:

$$\theta(i+1) = mod(\theta(i) + \Omega + \frac{K}{2\pi}Sin(2\pi\theta(i)), 1) \tag{1}$$

with θ being taken as modulo 1, and K and Ω being the control parameters. The standard circle map represents an area preserving chaotic map physically seen in systems such as the kicked rotator. However, the main feature of interest in the standard circle map are the variables θ, the angular phase normalized to unity and Ω, representing an angular frequency factor. Viewing this equation as a purely mathematical relation, as a first step, θ is written as $f_o t$ where f_o represents the normalized version of the angular frequency, given in the units of radians/sample, with a full scale range of $-\pi$ to π.

Also, the time factor t is set to one, representing one sample duration, between the ith and $i+1$th instants. The additive parameter Ω is rewritten as r where $r=f_2/f_1$ is the ratio between two normalized competing driving frequencies f_1 and f_2 and is the principal control parameter for the present work. The value of K is arbitrarily set to -2π in order to set the coefficient of the third term of the above equation to unity. Finally, the sinusoid $sin(2\pi\theta(i))$ is viewed as a mathematical function representing the input and is generalised to $V(2\pi f_o(i))$, or alternatively $V(f_o(i))$, with V representing the signal waveform fed to the input of the proposed chaotic system. Using these substitutions, the above equation is rewritten as

$$f_o(i+1) = mod(f_o(i) + r - V(f_o(i)), 1) \tag{2}$$

It is emphasized at this stage that, by making the various modifications to the standard circle map, its physical significance is altered considerably, and it now takes a new form represented by frequency variables and input signal dependence. In order to retain the consistency of the above equation, the various terms are normalized to π. First, the frequency f_o and the frequencies f_1 and f_2 are normalized to the radians/sample scale of $[-\pi, \pi]$. Finally, the term $V(f_o(i))$ is limited to π, i.e. 3.14 Volts by changing the modulus function from 1 to π. It will be later seen from Fig. (3) that the value of 3.14 V, comprehensively encompasses the linear and saturation operating regions of the transistor, as well as forms a convenient normalizing factor yielding effective integration of the frequency and voltage terms. At this point, it is observed that the f and V terms of the above equation are merely reduced to normalized mathematical numbers. Thus, the normalized version of the above equation, with the f and V terms limited to π using a modulus function is given as follows:

$$f_o(i+1) = mod(f_o(i) + \frac{f_2}{f_1} - V(f_o(i)), \pi) \tag{3}$$

This equation is the key iterative map of the present work.

Here the f_o terms denote the output frequencies, whereas f_1 and f_2 denote the frequencies of the input (driving) signals. $V(f_o)$ denotes the input signal waveform employed in the chaotic system. The salient features of the above mentioned iterated function are threefold, enumerated as follows:

1. The nonlinearity, provided by the modulus function represents the switching operation, which can be physically realized using a transistor operating in the cutoff and saturation regions [9].
2. The control parameter $r=f_2/f_1$ is an additive parameter and determines when the system transits from order to chaos and vice versa.

3. The $V(f_o)$ introduces a signal dependence, thus enabling the controlling of chaos by changing the waveform used as input. For instance, in the case of sinusoidally driven system, $V(f_o)$ becomes $sin(f_o(i))$ which can be decomposed into a power series containing the odd powers of $(f_o(i))$. Thus, the signal dependance introduces nonlinearity in addition to the system nonlinearity obtained by the switching function [9].

The bifurcation plot for a sinusoidal input $V(f_o(i))=sin(f_o(i))$ is given in Fig.(1).
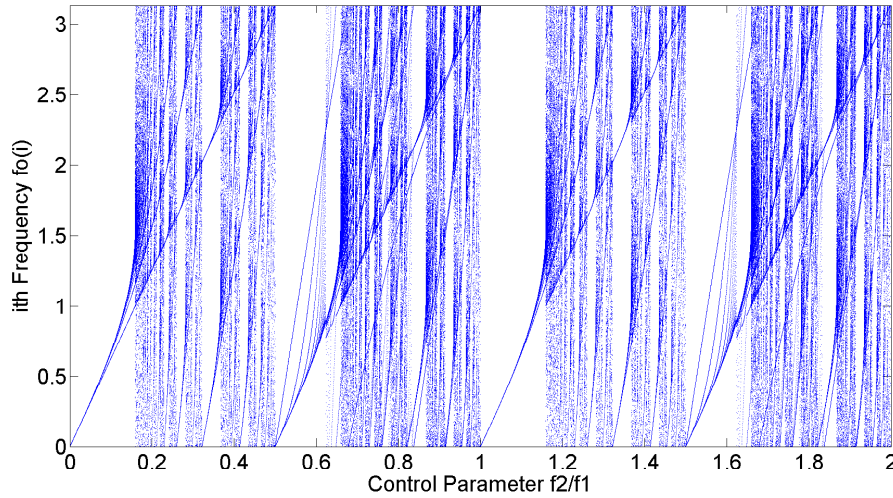
Figure 1: Bifurcation Diagram of the chaotic system with a sinusoidal input

From the diagram, two inferences stand out:

- The bifurcation pattern repeats itself with a period of 1.

- The control values close to integers (1,2,...) and half-integers (0.5, 1.5,...) give rise to order whereas non integral ratios such as 0.22 or 0.41 give rise to chaos.

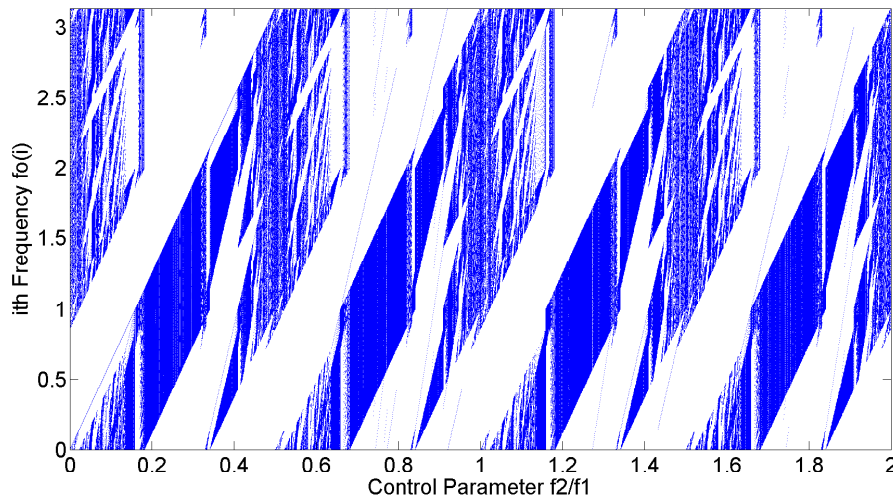A similar bifurcation diagram is plotted for square wave input, and is shown in Fig.(2).

Figure 2: Bifurcation Diagram of the chaotic system with a square wave input

The square wave bifurcation diagram shows chaotic behavior for a larger set of values of control parameter r compared to the sinusoid. A possible reason for this behaviour is that the square wave inherently contains a wide range of frequency

components, and thus allows for a more intricate interrelationship between various frequency components, as described by the iterative map of Equation 3.

The bifurcation plots clearly describe the behavior of the proposed chaotic system for various values of the control parameter r for typical inputs such as sinusoid and square.

3. Design and Implementation of the Chaos Generator

As highlighted in the previous section, the principal components of the proposed chaotic system are threefold - a switching element, frequency based control parameter and driving waveform. The first component is implemented in the present work using a single NMOSFET and the last two components are implemented using two driving signals fed to the gate and source terminals of the MOSFET [24, 11]. The driving signals are generated using ring oscillators. Thus, the implementation of the Ring Oscillators coupled to an NMOSFET, takes cue from Equation 3, representing the three terms of that equation 'in principle' by the three above mentioned elements.

These two elements - the MOSFET and the ring oscillator are described as follows. The whole implementation is carried out using Microwind, a deep submicron VLSI layout design software using a 180nm CMOS technology [10]. The device parameters and equations employed in the Microwind implementation are obtained from BSIM4 modeling [11].

3.1. Nonlinear Behavior of the NMOSFET

The primary source of nonlinearity for the generation of the proposed chaos is a switching element, and this is implemented using a MOSFET transistor [9, 10, 11, 12]. All the MOSFETs used in the present work are designed using a length of 200nm and a width of 600nm. This is achieved by selecting a length-width combination of $2\lambda \times 6\lambda$, where λ is the feature size, chosen in the 180nm technology to be 100nm. The nonlinearity of a MOSFET arises from two independent factors, described as follows.

The first factor is the the nonlinear dependence of the drain current I_d on the drain voltage V_D and the gate voltage V_G, valid for the nonlinear point between the linear and saturation regions [25, 26].

$$I_d = \frac{\mu_n Z C_i}{L}\left[\left(V_G - V_{FB} - 2\psi_f - \frac{V_D}{2}\right)V_D - \frac{2}{3}\frac{\sqrt{2\epsilon j_s q N_a}}{C_i}\left[(V_D + 2\psi_f)^{1.5} - (2\psi_f)^{1.5}\right]\right] \quad (4)$$

Here μ_n denotes the electron mobility, C_i the intrinsic capacitance, V_{FB} is the flat band voltage, j_s is the current density, q is the charge, N_a is the acceptor concentration, ψ_f denotes the work function, L denotes the channel length and Z denotes the channel width, both of which are the key transistor geometry parameters [26].

In order to study the I_d-V_D nonlinearity, the output characteristics of a $200nm \times 600nm$ NMOSFET are obtained from Microwind for various V_G values and are plotted in Fig. (3).
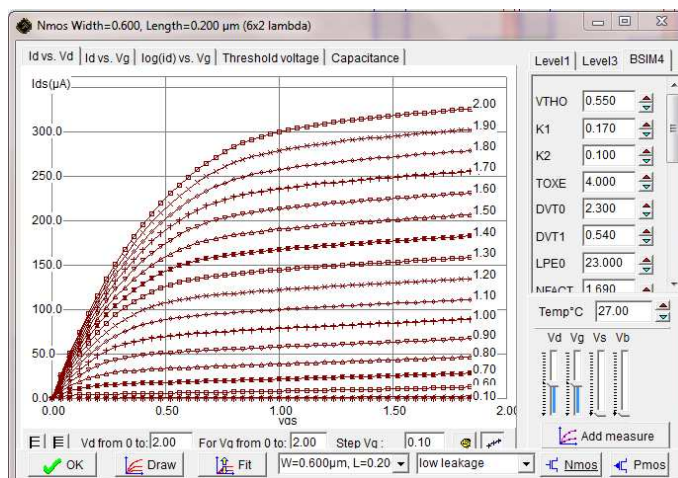

Figure 3: Output Characteristics of the NMOSFET as obtained from Microwind

The second factor contributing to the MOS nonlinearity is the Non-Quasi Static (NQS) charge model of the MOS channel relevant at high frequencies, which states that the channel of a MOSFET can be modeled as a nonlinear transmission line [12]. An illustration of the NQS model applied to the NMOSFET along with the drain, gate and source capacitances is shown in Fig.(4). This leads to the equivalent representation of the nonlinear transmission line by an

Elmore resistance [12]. This resistance is length dependant, which indicates the effect of wiring and transistor geometry in the proposed design. The equivalent circuit of Fig.(4), with the Elmore resistance denoted by 'Re' is shown in Fig.(5). The dependance on the Elmore Resistance on the gate-source voltage V_{gs} is given as follows:

$$Re = \frac{L_{eff}}{10\mu_{eff}W_{eff}C_{ox}(V_{gs} - V_{th})} \tag{5}$$

where μ_{eff} is the effective carrier mobility, L_{eff} and W_{eff} denote the effective channel length and width of the NMOS transistor, C_{ox} denotes the oxide layer capacitance and V_{th} is the threshold voltage of the transistor.
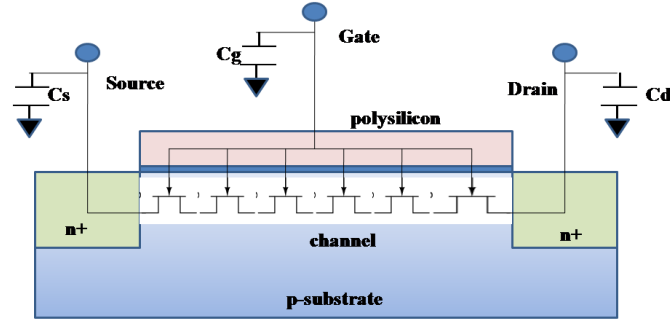

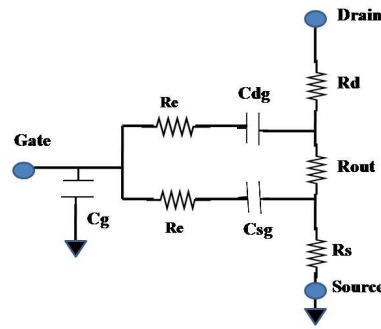Figure 4: Non-quasi static representation of a NMOS channel

Figure 5: Equivalent circuit of non quasi static channel effect

The significance of the application of this Elmore Resistance to the Non-Quasi Static model is that the NQS Relaxation time τ depends on a diffusion component $\tau_{diffusion}$ dominant in the subthreshold region of operation, and a drift component τ_{drift} valid in the strong inversion region, with the relation given as follows:

$$\frac{1}{\tau} = \frac{1}{\tau_{diffusion}} + \frac{1}{\tau_{drift}} \tag{6}$$

with the two components of τ given by the following expressions

$$\tau_{diffusion} = \frac{qL_{eff}^2}{16\mu_{eff}kT} \tag{7}$$

$$\tau_{drift} = ReC_{ox}W_{eff}L_{eff} \tag{8}$$

with q representing the charge and T representing temperature. The $1/\tau$ based relation is *ipso facto* a frequency oriented relation, and establishes the frequency-oriented charge transport mechanism of the transistor channel. This intuitively suggests how a single transistor can in its natural behavior generate frequency-dependent chaos.

5

3.2. Design of the Chaos Generator

As seen from the iterative map mentioned above, the MOS switching nonlinearity has to be triggered by driving signals, whose waveforms and frequencies also affect the chaos generated. In order to accomplish this, two driving signals A and B are fed, one each to the gate and source terminals of the MOSFET. The ratio of the frequencies of the driving signals f_1 and f_2 determine the control parameter, $r=f_2/f_1$.

A Ring Oscillator is a resonator-less Oscillator formed by connecting in a closed loop, an odd number of inverters [9]. The transfer characteristics for a single CMOS Inverter stage as obtained from Microwind is shown in Fig. (6). As seen in the figure, the obtained transfer characteristics have been fitted with a sigmoid of the following form, where Vx and Vy represent the Input (Common Gate) and Output side Signals respectively. From the plot, it can be seen that the key nonlinear transition points of the transfer curve lie at around 0.7V and 1V of the input voltage Vx.

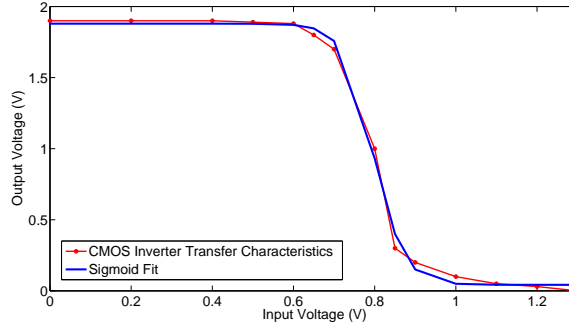$$Vy = 0.0421 + \frac{1.8372}{1 + 10^{-11.7657(0.7977 - Vx)}} \tag{9}$$

Figure 6: The transfer characteristics of a CMOS Inverter as obtained from Microwind (red), with a sigmoid fit for the same (blue)

Since in odd number of inverters, the output of the last stage is a complement of the input to the first stage, this creates a theoretically endless cycle of instability, witnessed by the continuous alternating between low and high states. The time period of the ring oscillator output is given by the relation

$$T = 2MT_d \tag{10}$$

where M denotes the number of stages and T_d is the delay of each stage.

In a ring oscillator, the key variables facilitating tunability variables are the number of inverter stages and the power supply. Thus, in a given technology node, a ring oscillator with the smallest number of stages, three, ensures the maximum frequency obtainable in that technology. However, in order to achieve the tunability advantage mentioned in the previous sections, it is necessary to alter the number of stages of the ring oscillator, thus altering its output frequency. This can be accomplished by designing a 'programmable' ring oscillator which can switch between various odd numbers of stages. One such example of a ring oscillator which can switch between three, five and seven stages is conceptually illustrated in Fig. (7). In the present work, 180nm technology is used with the power supply set to 2V. The schematic of a ring oscillator constructed with three CMOS inverter stages are shown in Fig. (8) respectively.

The Microwind implementation of the ring oscillator is carried out, and the output waveform is obtained with an amplitude of 1.5V. It is noteworthy that the amplitude of the voltage waveform is around 1.5V, thus clearly spanning the cutoff and saturation regions, as visible from the characteristics of Fig. (3). The peak frequency obtained as 5.53GHz thus forms the value of f_2, and the ring oscillator output A forms the input to the source terminal of the NMOSFET for chaos generation.

In a similar fashion to the one mentioned above, another ring oscillator with five inverter stages is used to form the second driving input B. As can be seen, the peak frequency of this signal and hence the controlling frequency f_1 is 3.29GHz. The frequency ratio thus obtained is $f_2/f_1 = 1.68$ with a mantissa value of 0.68, and as seen from the bifurcation plots of Fig.(1) and Fig.(2), this value of r certainly gives rise to chaos.

In any given technology, the requirement that the two driving signals need to form a non-integral frequency ratio, coupled with the proposed design consisting of a single switching NMOS driven by two ring oscillators with three and five stages ensure that the two driving frequencies are the highest obtainable in that technology and thus the frequency dependant chaos obtained is of the highest frequency possible in that technology [9]. For this reason, this design is emphasized in the present work.
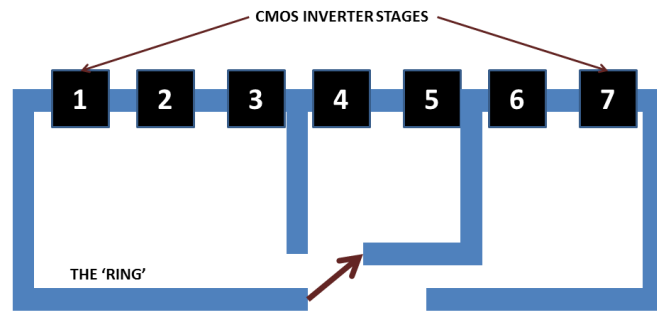
6

Figure 7: Block Diagram of a 'programmable ring oscillator' indicating the ability to switch between three, five or seven stages output
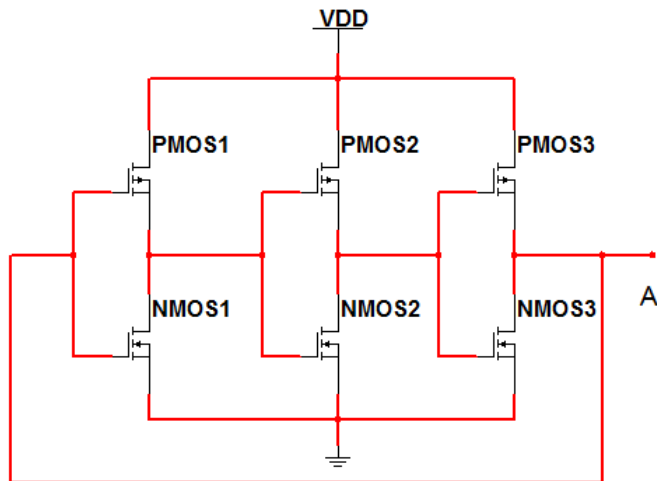

Figure 8: Schematic of a three stage ring oscillator

The two elements of NMOSFET and ring oscillator detailed above are combined with the two ring oscillator outputs A and B being fed to the source and gate terminals of the NMOSFET respectively. The schematic of the proposed chaos generator is shown in Fig. (9) and the corresponding layout is shown in Fig. (10).
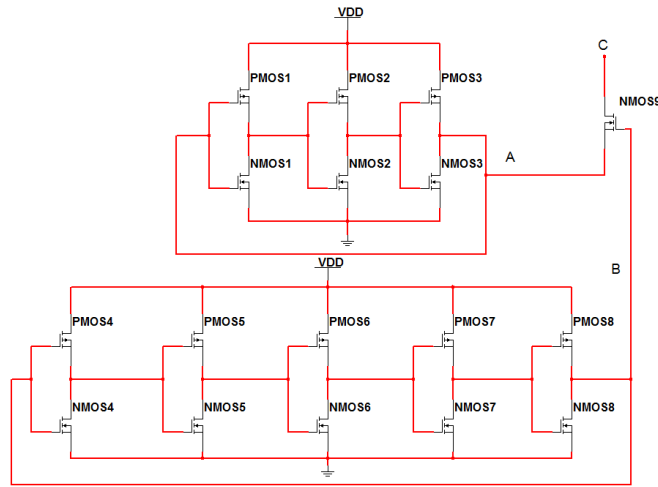

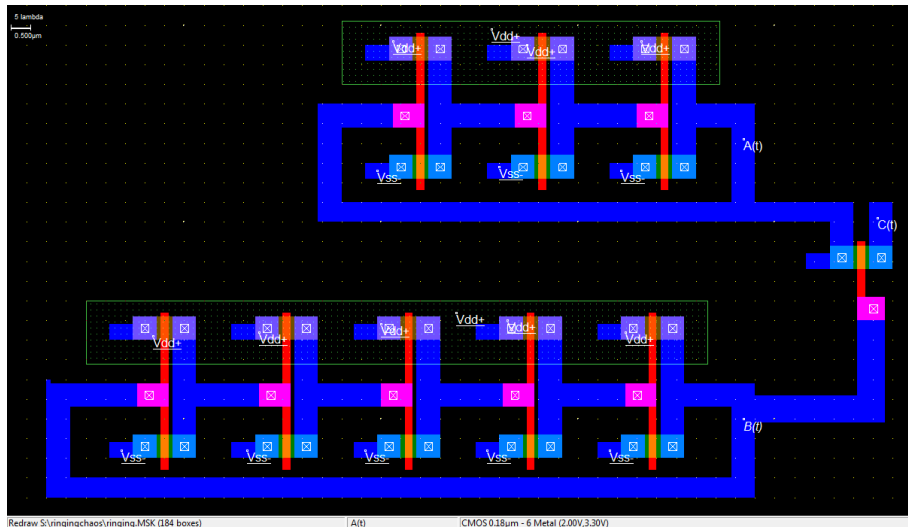Figure 9: Schematic of the Chaos Generator

Figure 10: Layout of the Chaos Generator

4. Characterization of the Chaotic Output

The implementation of the layout as shown in Fig. (10) in Microwind yielded the output voltage waveform C of the chaos generator as shown in Fig. (11). The corresponding FFT spectrum is as shown in Fig. (12). This spectrum clearly shows a more pronounced dominance (about 30dBuV) of harmonics in the 1-10GHz range. These harmonics clearly assert the nonlinearity induced by the switching operation of the transistor. The netlist of the circuit, given in the appendix, shows significant values of wiring and other related parasitic capacitances and coupling effects. It is noteworthy that these parasitics add to the chaotic behavior of the circuit by interacting with the non quasi static model of the transistor as explained in the previous section. Thus, the present design inherently allows for parasitic behavior, thereby preventing the use of excessive filtering, guard rings etc., thus maintaining a low power dissipation. However, a more thorough investigation into synchronization effects between ring oscillators as well as phenomena such as injection locking and phase noise and their effect on the generated chaos is required.
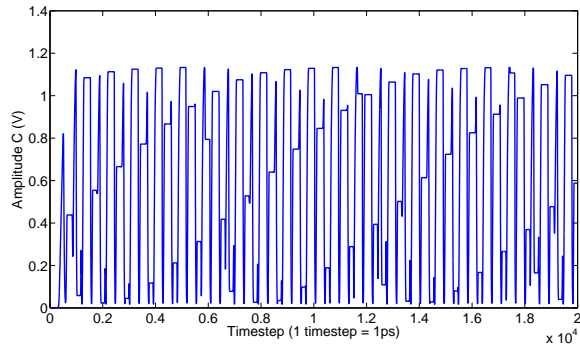
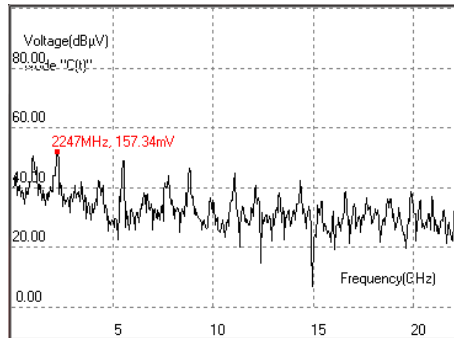Figure 11: Voltage Waveform output of the chaos generator

Figure 12: FFT Spectrum of the output of chaos generator

4.1. Phase Portrait

One of the classical analysis techniques for a chaotic signal is to plot its phase portrait. This portrait, depicting the time derivative of a signal (dV/dt) as a function of the signal (V) illustrates the dynamics of the signal in the phase space. This describes the stability aspects of the chaotic system behavior and points of stability around which the system revolves, qualitatively serving as a tool to assess various chaotic parameters such as sensitivity and ergodicity [4, 3]. The phase plane of the generated chaotic signal C is shown in Fig. (13). The phase portrait illustrates an ornamental pattern, clearly describing the chaotic behavior of the proposed system.
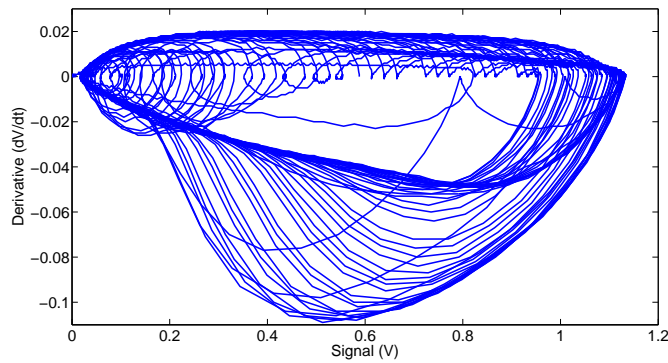

Figure 13: Phase Portrait of the generated chaos

4.2. Lyapunov Exponent (LLE)

The chaotic nature of the signal C is assertively established by calculating the largest Lyapunov Exponent (LLE), a measure of a system's sensitive dependence on initial conditions [27, 28]. Rosenstein's algorithm is used to compute the

Lyapunov Exponents λ_i from the voltage waveform, where the sensitive dependence is characterized by the divergence samples $d_j(i)$ between nearest trajectories represented by j given as follows, C_j being a normalization constant:

$$d_j(i) = C_j e^{\lambda_i (i\delta t)} \tag{11}$$

The Largest Lyapunov exponent thus obtained for the signal C is 8.23, the positive value proving the fact that the signal is indeed chaotic.

4.3. Fractal Dimension (D)

The chaotic/fractal nature of the signal C is further confirmed by computing the fractal dimension, using the Minkowski Bouligand Box Counting Method [29]. In this method, various square 'boxes' of different sizes e are formed and for each size e, the number of boxes $N(e)$ required to cover the entire set is computed [29]. The fractal dimension D is then given by

$$D = \lim_{e \to 0} \frac{log(N(e))}{log(e)} \tag{12}$$

For the output waveform of C as shown in Fig.(11), the fractal dimension is obtained as 0.661, indicating the presence of self-similarity in the generated signal.

4.4. Kolmogorov Entropy (K_2)

Finally, the worthiness of the generated signal as a potential candidate as a carrier for secure communications can be established by ascertaining the amount of information that can be carried by the signal. This is precisely quantified by the Kolmogorov Entropy, a statistical measure of the uncertainty of the signal [27, 8, 1]. By assigning each of the N quantifiable states of the amplitude of C as an event i, the Kolmogorov Entropy K_2 obtained depends on their probabilities p_i according to the relation

$$K_2 = -\sum_{i=1}^{N} p_i \log p_i \tag{13}$$

Since the chaotic output waveform is a continuously varying amplitude, a very high value of N such as 100000 is selected as the number of quantifiable states. Thus, the presence of each of the N states is viewed as an event p_i. The K_2 value thus obtained is 3.96 bits/symbol, clearly testifying to the information carrying capacity of the generated chaotic signal C.

4.5. Characterization of Power Dissipation and Effect of Noise

A significant aspect of the implementation of any chaotic system in electronics is the power dissipation of the circuit, which ultimately decides its efficiency. In the present work, since ring oscillators are used, the main variable is the supply voltage used. Thus a plot of the power dissipation observed for various values of supply voltage is shown in Fig. (14). As can be seen, the power dissipation rises to a maximal value of 0.5mW for a supply voltage of around 1V. On either
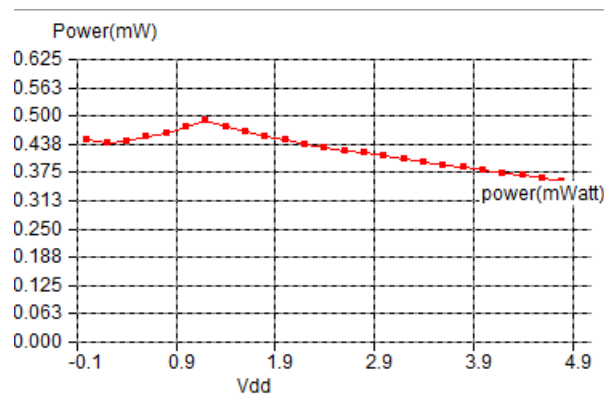

Figure 14: Power Dissipation as a function of Supply Voltage

side of this point, the power dissipation decreases. The peak power at the supply voltage value of 1V could possibly be attributed to the nonlinear transition point observed in the CMOS inverter transfer curve of Fig. (6), since the limiting

10

of supply voltage to 1V limits the peak output of the inverter to 0.9-1V, which is known as a point where the transistor draws more current, increasing power dissipation [9]. This, in turn drives the NMOSFET at the saturation region. The very low power dissipation obtained is owing to the extremely simple circuit used [10].

The presence of noise in the MOS transistor, the principal component of the ring oscillator circuit inevitably leads to time domain jitter and amplitude variation based noise in practice. However, the low power consumption and dissipation as described above mitigates this effect to a certain extent. In order to characterize the effect of noise on the nature of the chaotic output, the relevant noise parameters in BSIM4 such as thermal, shot and flicker noise models were enabled. [9]. It is seen that with these models turned on, the total noise generated at the output stage corresponds to a Signal to Noise Ratio (SNR) of 24dB. For the initial case of $r = 1.68$ with ring oscillators of three and five stages, the output signal spectrum and the phase portrait including noise effects are plotted in Fig. (15) and Fig. (16). It is seen that the phase portraits and FFTs and hence the nature of chaos are not significantly altered due to noise.
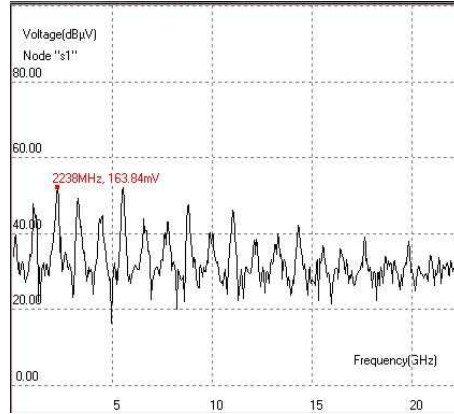

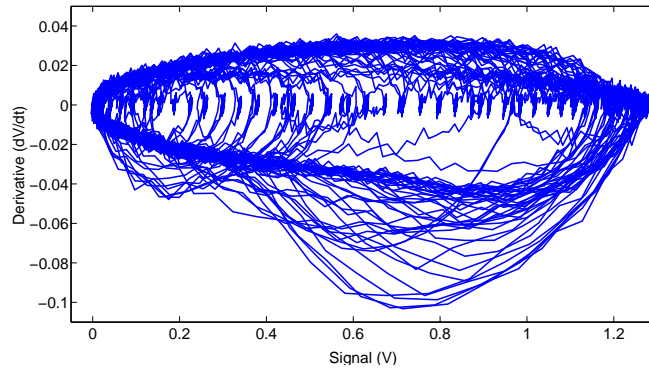Figure 15: The FFT spectrum of the chaotic output signal in the 24dB noise included model

Figure 16: Phase Portrait of the chaotic output signal in the 24dB noise included model

4.6. Variation of Frequency

According to the basic premise of the proposed frequency dependant chaos, as witnessed by the iterative map and bifurcation diagrams described earlier, the nature of the chaos generated depends on the frequency of the driving signal. In the case of ring oscillators, the direct way of altering the frequency is by changing the number of inverter stages used. In keeping with the rule of having an odd number of inverters, various combinations of inverter stages including three, five, seven and nine are implemented, and the corresponding parameters of LLE, D and K_2 are tabulated. From the table, it is observed that the frequency of the driving signals indeed affect the nature of chaos generated.

One interesting observation from the table is that for the Configurations of 3 stages and 5 stages and for the configuration of 5 stages and 9 stages, the values of K_2 (3.96 and 3.91 respectively) and LLE obtained are very similar (8.23 and 8.07 respectively). This establishes the inference that even though the base frequencies (f_1) are different for both cases (3.29 GHz and 1.98 GHz), the nature of the chaos generated is nevertheless very similar owing primarily to the similarity in the r values in the two cases (1.68 and 1.66). A similar observation can also be made for the 5 stages-7 stages

Table 1: Effect of Driving Signal Frequency on the Generated Chaos

Stages of A	Stages of B	f_2 (GHz)	f_1 (GHz)	Ratio r	LLE	D	K_2 (bits/sym)
3	5	5.53	3.29	1.68	8.23	0.661	3.96
3	7	5.53	2.54	2.17	7.89	0.661	3.87
3	9	5.53	1.98	2.79	6.75	0.632	3.65
5	7	3.29	2.54	1.29	6.35	0.632	3.62
5	9	3.29	1.98	1.66	8.07	0.661	3.91
7	9	2.54	1.98	1.28	6.46	0.632	3.63

and 7 stages-9 stages cases as well. This indicates that the properties of the chaos generated are primarily determined by the choice of r, the control parameter, as had been initially formulated. This property of the proposed circuit enables one to choose an appropriate base frequency and hence, number of ring oscillator inverter stages with minimal power dissipation, while not altering the nature of the generated chaos as long as the desired ratio r value is maintained.

In addition to the frequencies of the driving signals, the power supply of the chaos generator, by itself also has an influence on the output frequency of the ring oscillators and thus the chaos generated [9]. This variation of the output frequency is characterized in Fig. (17).
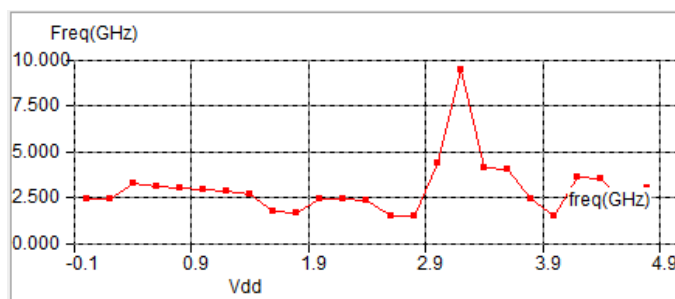

Figure 17: Dependance of the Output Frequency on Supply Voltage

It is seen that for the most part, the frequency varies about the range of 2-4GHz, except during a supply voltage of 3.1V, where the frequency surges upto nearly 10GHz. A possible explanation for this is the normalization and modulus based limiting of the voltage term to π, as in Equation 3. However, since the supply voltage value of 3.1V lies well above any significant region of transistor operation (linear, saturation or cutoff), this region of operation may not be a reliable and consistent one.

5. Conclusion

A frequency dependent iterative map is proposed based on the standard circle map and characterized using bifurcation plots. It is seen that the proposal of a frequency dependent rather than amplitude dependent chaos promises two crucial advantages - easy tunability, thanks to the driving signals and simplicity of implementation. Deep Submicron VLSI implementations in SPICE are carried out using 180nm technology. For the two driving signals, ring oscillators comprising of three and five stages of CMOS inverters are used. The nonlinearity is obtained from the switching behavior of a single NMOS transistor. The generated chaos is then characterized qualitatively using waveform, spectrum and phase portraits, and quantitatively using Kolmogorov Entropy, Lyapunov Exponent and Fractal Dimension. Finally, the effect of number of stages and the power supply on the nature of chaos generated is also investigated.

Of further work in this direction, the primary step would be to investigate and characterize the nature of chaos and its dependence on loading effects for various kinds of inductive and capacitive loads. Nevertheless, the simplicity of the circuitry and the easy tunability obtained by using a signal dependant (frequency) control parameter, coupled with the low value of power dissipation obtained form the novelties of the present work. The generated chaotic signal finds immense applications in communnications and computing such as secure communications, encryption and random number generators.

References

[1] G. B. Giannakis, F. Bach, R. Cendrillon, M. Mahoney,J. Neville, *Signal Processing for Big Data*, IEEE Signal Processing Magazine, **31**, 15-16 (2014).

[2]   M. Hilbert, *How much of the global information and communication explosion is driven by more, and how much by better technology?*, Wiley Journal of the Association for Information Science and Technology, **65**, 856-861 (2014).

[3]   M. Ausloos, M. Dirickx, *The Logistic Map and the Route to Chaos: From the Beginnings to Modern Applications*, (Springer, US, [2006]).

[4]   S. H. Strogatz, *Nonlinear Dynamics and Chaos: With Applications to Physics, Biology, Chemistry, and Engineering* ,(Westview Press, Cambridge, 2008).

[5]   E.Bilotta and P.Pantano, *A gallery of Chua attractors*, (World Scientific, Singapore, 2008).

[6]   M. H. Jensen, P. Bak, T. Bohr, *Complete Devil's Staircase, Fractal Dimension, and Universality of Mode- Locking Structure in the Circle Map*, Phys. Rev. Lett. **50**, 1637 (1983).

[7]   M. F. Barnsley, A. D. Sloan, *Chaotic Compression*, Computer Graphics World, **3** (1987).

[8]   K. E. Barner and G. R. Arce, *Nonlinear Signal and Image Processing: Theory, Methods, and Applications*, (CRC Press, U.S, 2003).

[9]   B. Razavi, *RF Microelectronics*, (Prentice Hall, US, 2011).

[10] J. P. Uyemura, *Chip Design for Submicron VLSI: CMOS Layout and Simulation*, (Thomson/Nelson, US, [2006]).

[11] W.Liu, *BSIM 4.0.0 MOSFET Model: User's Manual* (Electronics Research Laboratory,US, [2000]).

[12] M.Chan, K.Hui, C.Hu, P.K.Ko, *A robust and physical BSIM3 non quasi static transient and AC small signal model for circuit simulation*, IEEE Transactions on Electron Devices. **45**, 834 (1998).

[13] Y. Hosokawa, Y. Nishio, A. Ushida, *Chaotic Circuit Using Two Simple Ring Oscillators Coupled by Diodes*, Proc. NOLTA, **99**, 107, (1999).

[14] Y. Hosokawa, Y. Nishio, A. Ushida, *Analysis of Chaotic Phenomena in Two RC Phase Shift Oscillators Coupled by a Diode*, IEICE Transactions on Fundamentals, **E84-A**, 2288, (2001).

[15] Y. Hosokawa, Y. Nishio, *Simple Chaotic Circuit using CMOS Ring Oscillators*, Int. J. Bifurcation Chaos, **14**, 2513, (2004).

[16] Y. Nishio, A. Ushida, *Spatio-temporal chaos in simple coupled chaotic circuits*, IEEE Trans. Circuits and Systems 1, **42**, 678, (1995).

[17] I. Cicek, G. Dundar, *A hardware efficient chaotic ring oscillator based true random number generator*, IEEE ICECS, **18**, 430 (2011).

[18] I. Cicek, G. Dundar, *A chaos based integrated jitter booster circuit for true random number generators*, ECCTD, **1**, 8 (2013).

[19] R. Gilmore and M. Lefranc, *The Topology of Chaos*, (Wiley,US, [2002]).

[20] J. M. T. Thompson and H. B. Stewart, *Nonlinear Dynamics and Chaos* (Wiley,UK, [2002]).

[21] V. I. Arnold, *Small Denominators I. Mappings of the circumference onto itself*, Am. Math. Soc. Transl, **46**, 213-284 (1965).

[22] M. R. Hermann, *Mesure de Lebesgue et nobre de rotation (Geometry and Topology)*, (Springer,Germany, [1977]).

[23] R. S. Mackay and C. Tresser, *Some flesh on the skeleton: the bifurcation structure of bimodal maps*, J. Phys. Lett., **45**, L741-L746 (1984).

[24] F. Balestra, *Nanoscale CMOS: Innovative Materials, Modeling and Characterization* (Wiley,US, [2013]).

[25] M. E. Inchiosa, A. R. Bulsara, A. D. Hibbs, B. R. Whitecotton, *Signal Enhancement in a Nonlinear Transfer Characteristic*, Phys. Rev. Lett. **80**, 1381 (1998).

[26] B. G. Streetman and S. K.Banerjee, *Solid State Electronic Devices*, (PHI, U.S, [2006]).

[27] R. G. James, K. Burke, J. P. Crutchfield, *Chaos forgets and remembers: Measuring information creation, destruction, and storage*, Int. J Bifurcation Chaos. **378**, 2124 (2014).

[28] M. T. Rosenstein, J. J. Collins, C. J. De Luca, *A practical method for calculating largest Lyapunov exponents from small data sets*, Physica D, **65**, 117, (1993).

[29] P. Maragos, F. K. Sun, *Measuring the fractal dimension of signals: morphological covers and iterative optimization*, IEEE Trans. Signal Processing, 41, 108-121 (1993).